Journal of Structural Geology Vol 13, No 9 pp 1061 to 1078, 1991
Printed in Great Britain

0191-8141/91 $03 00+0 00

The role of stress in ductile deformation

RUUD WEIJERMARS

Hans Ramberg Tectonic Laboratory, Institute of Geology, Uppsala University, Box 555
S 751 22 Uppsala, Sweden

(Received 1 December 1989, accepted in revised form 5 February 1991)

Abstract—The concept of progressive ductile deformation has previously been discussed mainly in kinematic terms. Little attention has been paid to the principal stresses that control the formation of ductile deformation patterns. Many deformation patterns of rocks may have been created in a stress field of stable orientation. An equation derived here directly links the orientation of the major axis of deviatoric stress to the stretch and rotation components of plane isochoric deformation in isotropic rocks. Estimations of rotation and stretch of finite strain ellipsoids may therefore aid the recovery of palaeostress axes using a nomogram introduced here.

The inclination of the major principal deviatoric stress axis with respect to a reference plane controls both the particle movement paths and mode of progressive deformation. The deformation tensor, obtained by integrating the rate of displacement or velocity gradient equations, is first expressed in time dependent terms comprising only the normal and shear components of the strain rate tensor. Mohr's equations of stress can then be used to link strain rates to the major principal stress responsible for them. The rate of progressive deformation is determined by the rheology of the deforming rocks and the magnitude of the deviatoric stress. This derivation yields a time dependent deformation tensor which is expressed in terms of the dynamic viscosity and the magnitude and orientation of the major deviatoric stress with respect to a reference plane. The significance of this deformation tensor is illustrated by forward modelling using computer graphics. These allow the progressive deformation of a unit volume of rock in response to deviatoric stresses of various stable orientations to be visualized.

INTRODUCTION

STRUCTURAL geologists have developed techniques to map, methods to display and jargon to describe, the *geometry* of deformation patterns observed in rocks. The structural features of particular terrains are sometimes used to reconstruct their *kinematic* or tectonic history. However, this traditional, descriptive approach of structural geology does not address fundamental questions concerning the *dynamics* of deformation. For example, "Never talk about stresses, all you see in rocks is a state of finite strain which may result from any deformation history", is a common statement repeatedly emphasized by the community of structural geologists.

And yet, many geologists wonder: Why is the geometry and scale of folds, boudins, mullions and shear zones so variable? Why do these structures occur at all? Field geologists therefore commonly resort to mental models, invoking mechanisms that could have led to the structures observed in the field. These models usually prompt allegations about the orientation of the principal stresses. Such mind experiments are often a drastic simplification as they extrapolate from familiar dimensions and condense the factor of time while animating the frozen movements found in rock structures (cf. Kuenen 1965). The accuracy of mental models could therefore benefit from investigating and quantifying the relationship between stress and strain in elementary models. It is a task of modern structural geology to provide this background knowledge.

The relationship between stress and strain is complex because finite strain can only be determined by time integration when the vorticities and strain rates are known. This work shows how both the flow geometry and mode of progressive deformation are entirely controlled by the inclination of the principal deviatoric stress axis relative to a stable reference plane fixed to a physical boundary of the deforming rock volume. Until now, this relationship between mode of deformation and orientation of the deviatoric stress had only been recognized for two specific cases. These are progressive pure shear and simple shear, for which the principal deviatoric stress is perpendicular to, and at 45° to, respectively, a fixed reference plane in the material. The deformation tensor introduced here allows determination of progressive deformation sequences for any stable orientation of the stress axes within the plane of flow. Additionally, the rate of accumulation of finite strain can be predicted knowing the magnitude of the vorticity and strain rate as these are controlled by the magnitude of the stress and the effective viscosity of the system.

Progressive deformation of circular markers has previously been visualized by Pfiffner & Ramsay (1982) who obtained their results in an instructive approach superposing small increments of strain and rotation. Ramberg's (1975a,b) earlier treatment of progressive deformation was less illustrative but theoretically more sophisticated because it discussed the development of finite strain in terms of strain rate and rotation rate, both at steady state. The type of progressive deformation and the associated pattern of particle movement paths (streamlines) appeared to be critically dependent on the relative magnitude of vorticity and strain rate (Ramberg 1975a,b). This was in agreement with previous developments in fluid mechanics where similar streamline patterns were calculated by integrating the velocity gradient tensor for arbitrary ratios of vorticity and strain rate (Giesekus 1962). Consequently, finite deformation is predictable but only if the history of strain rate and vorticity contributions is fully known, and preferably these are at steady state.

Two distinct classes of progressive deformation in planar flows were implied in Ramberg's (1975a,b) analyses, causing pulsating and non-pulsating strains. Introduction of Truesdell's (1953) kinematic vorticity number (W_k) into geological literature allowed indexing of deformations, where *finite* strain oscillates or pulsates ($1 < W_k \leq \infty$) and accumulates monotonically ($0 \leq W_k \leq 1$), respectively (Means *et al.* 1980). McKenzie (1979) had previously expressed the deformation tensor in terms of vorticity and strain rate, and indicated for which ratios oscillatory and non-oscillatory strains occur. Oscillatory progressive strains were also included in Pfiffner & Ramsay (1982, cf. Ramsay & Huber 1983), but without reference to the kinematic vorticity number. It is worth noting that Giesekus (1962) also used a parameter ρ—identical to the kinematic vorticity number—for distinguishing the closed and hyperbolic flow paths, which Ramberg (1975a,b) later connected to pulsating and non-pulsating strains.

The kinematic vorticity number is now increasingly used as a measure for *non-coaxiality* of progressive deformation (cf. Ghosh 1987). But this is not a unique measure for characterizing the progressive deformation history. This is because it characterizes only the streamline pattern. It includes no information concerning the boundary conditions and initial shape and orientation of the deforming volume with respect to that flow pattern. Different progressive deformations leading to thinning and thickening of the same layer may have similar W_ks (see later). The kinematic vorticity number is therefore an incomplete measure of progressive deformation. W_k is still useful to distinguish pulsating and non-pulsating strains, but the specific mode of non-oscillatory strain is better characterized by the orientation of the deviatoric stress axes with respect to a particular reference plane.

Current ambiguities about the role of stress and the importance of the kinematic vorticity number could be resolved by invoking basic concepts of fluid mechanics and continuum mechanics. Although structural geology is a practical, field oriented science, it may be worthwhile to start from basic principles if this promises a better understanding of our field data. The discussion below therefore introduces the stream function for homogeneous plane deformation and demonstrates how it characterizes the pattern of particle movement paths. The flow field may also be characterized by a non-dimensional parameter ζ contained in the particular stream function derived below. However, the mode of progressive deformation depends upon the boundary conditions (viz. stress orientation) and therefore specification of the mode of flow is insufficient to characterize the deformation history.

STREAM FUNCTION OF HOMOGENEOUS PLANE STRAIN

Like previous studies, this investigation of the systematics of progressive deformation is confined to ductile deformation patterns formed (1) in plane strain, (2) at steady-state and (3) without volume change. Additionally, the reference volumes considered are at a scale small enough to correspond to homogeneous deformation. The validity of these assumptions for creeping rocks will be retrospectively discussed in a later section.

The assumption of plane strain at steady state without volume change implies that the streamlines or particle movement paths controlling the deformation will remain within the plane containing the long and short axes of the strain ellipsoid. The entire suite of flow patterns possible in two dimensional flows giving homogeneous deformation structures is illustrated in Fig. 1. These flow patterns can be characterized by the following expression of velocity components $v(x,y,z)$ (cf. Mason 1977).

$$v_x = \gamma z \quad (1a)$$

$$v_y = 0 \quad (1b)$$

$$v_z = \zeta\gamma x, \quad (1c)$$

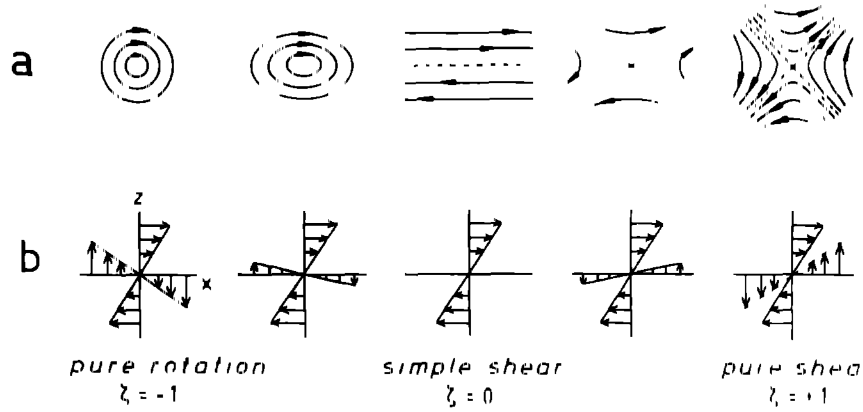

Fig. 1. Specific examples of two dimensional laminar flows represented by (a) streamlines and (b) velocity components. The flows can be characterized by the dimensionless parameter ζ, varying from −1 (rigid body rotation) to +1 (pure shear). After Mason (1977, fig. 1).

where ζ is a dimensionless scaling parameter varying between 1 and -1, and $\dot{\gamma}$ is the rate of shear. Familiar cases of progressive deformation occur for $\zeta = -1$ (pure rotation and no strain), $\zeta = 0$ (simple shear) and $\zeta = 1$ (pure shear). The ellipticity of oscillatory streamline patterns, expressed as the ratio of the short to the long axis, is given by the square root of $-\zeta$ (cf. Fuller & Leal 1981, equation 15).

It is more practical to express the flow field of Fig. 1 in terms of a stream function. This, by definition, automatically satisfies the conditions of continuity and the force balance equation of Navier-Stokes. The stream function therefore is a solution of the biharmonic function **lap lap** $\Psi = 0$, which is only equal to zero for incompressible flows as assumed here. The stream function cannot be determined from this general equation (as is sometimes suggested in geological literature) because the number of solutions is infinite. A stream function describing the flow spectrum for homogeneous plane strain is obtained here by making proper use of its definition as $v_x = \partial\Psi/\partial z$ and $v_z = -\partial\Psi/\partial x$. It can simply be recovered by integrating the velocity field equations:

$$\Psi = \int(\partial\Psi/\partial x)\,dx + \int(\partial\Psi/\partial z)\,dz + c$$
$$= \int v_x\,dz - \int v_z\,dx + c. \qquad (2)$$

The following stream function is obtained by integration of expression (2), using the velocity field equations (1a)–(1c) and dropping the integration constant c using the condition $\Psi = 0$ [m^2 s^{-1}] at $(x,z) = (0,0)$:

$$\Psi = (\dot{\gamma}/2)(z^2 - \zeta x^2) \qquad (3)$$

Streamlines similar to those in Fig. 1 can be mapped accurately by equating Ψ to a constant volumetric flow rate [m^2 s^{-1}, with unit vector in the y direction], using fixed values of ζ and an arbitrary $\dot{\gamma}$. Expression (3) is only valid for the particular orientation of the co-ordinate axes shown in Fig. 1. Although ζ is by definition related to this particular orientation of the reference frame, it may still be used to characterize streamline patterns in general because co-ordinate systems are arbitrary.

KINEMATIC VORTICITY NUMBER

Flowlines such as outlined in Fig. 1 can be used to predict patterns of progressive deformation arising after the insertion of passive deformation markers in such flows. Particle paths, streamlines, flowlines and streak lines will all be the same for the steady-state low Reynolds number flows studied here (cf. Tritton 1988). Flow markers will therefore deform by displacement along the streamlines. Figure 2 illustrates qualitative examples of progressive deformation for a unit square by streamline patterns for $\zeta = 1, 0.2, 0, -0.1, -0.3, -0.6$ and -1. It is important to realize that the progressive deformation of the square is not only determined by the streamline pattern, but also by its initial orientation with respect to the streamlines.

Current geoscience literature usually refers to the kinematic vorticity number W_k of progressive deformation (Means *et al.* 1980). This originates from a particular convention for decomposition of the velocity gradient tensor (Truesdell 1953, 1954, 1965, Truesdell & Toupin 1960). This non-dimensional number characterizes the relative importance of the principal strain rates ($\dot{e}_i$) and vorticity ($\dot{\omega}_i$) derived from the velocity gradient tensor L_{ij} of steady state flows (Truesdell 1953, p. 175, 1954, p. 107)

$$W_k = \frac{|W|}{[2(\dot{e}_1^2 + \dot{e}_2^2 + \dot{e}_3^2)]^{1/2}}, \qquad (4a)$$

where the magnitude of the vorticity vector $|W| = (\dot{\omega}_1^2 + \dot{\omega}_2^2 + \dot{\omega}_3^2)^{1/2}$. Note that the kinematic vorticity number as written here contains the principal strain rates and not the normal strain rate components of the strain rate tensor (see later).

The kinematic vorticity number for a general two-dimensional flow is less complex than in expression (4a). This is because the unchanged intermediate stretch axis (S_2) in any plane deformation always remains perpendicular to the plane of flow. The vorticity vector of plane (rotational) strains also will remain consistently perpendicular to the plane of flow. Consequently, any isochoric plane strain will have $\dot{\omega}_1 = 0$, $\dot{\omega}_2 \neq 0$, $\omega_3 = 0$, $\dot{e}_1 = -\dot{e}_3$, $\dot{e}_2 = 0$, $\dot{e}_3 = -\dot{e}_1$, assuming a convenient choice of the co-ordinate axes. Substituting these values in expression (4a) gives the kinematic vorticity number for a general two-dimensional flow:

$$W_k = |\dot{\omega}_2|/[2(\dot{e}_1^2 + (-\dot{e}_1)^2)]^{1/2} = |\dot{\omega}_2/2e_1| \qquad (4b)$$

It is worth noting that the relative magnitude of strain rate and vorticity may be visualized in Mohr diagrams (cf. Lister & Williams 1983, Passchier 1986, 1987, 1988, 1990).

Perhaps the most powerful property of the kinematic vorticity number is that it characterizes the geometry of particle movement paths (cf. Weijermars 1988b, fig. 5). The geometry of two-dimensional flow patterns is similar for all pairs of $(e_1, \dot{\omega}_2)$ which give the same kinematic vorticity number. It is therefore relevant to clarify the relationship between the kinematic vorticity number, W_k, stream function, Ψ, and scaling parameter, ζ.

The relationship between Ψ and W_k is straightforward since the magnitudes of $\dot{e}_1$ and $\dot{\omega}_2$ (or $\dot{\omega}_y$) are implied in Ψ. Components of the strain rate tensor can be obtained from the expressions:

$$\dot{e}_{xx} = \partial v_x/\partial x = \partial^2\Psi/\partial x\partial z \qquad (5a)$$

and

$$\dot{e}_{xz} = (1/2)[\partial v_x/\partial z + \partial v_z/\partial x] = \tfrac{1}{2}[\partial^2\Psi/\partial z^2 - \partial^2\Psi/\partial x^2]. \qquad (5b)$$

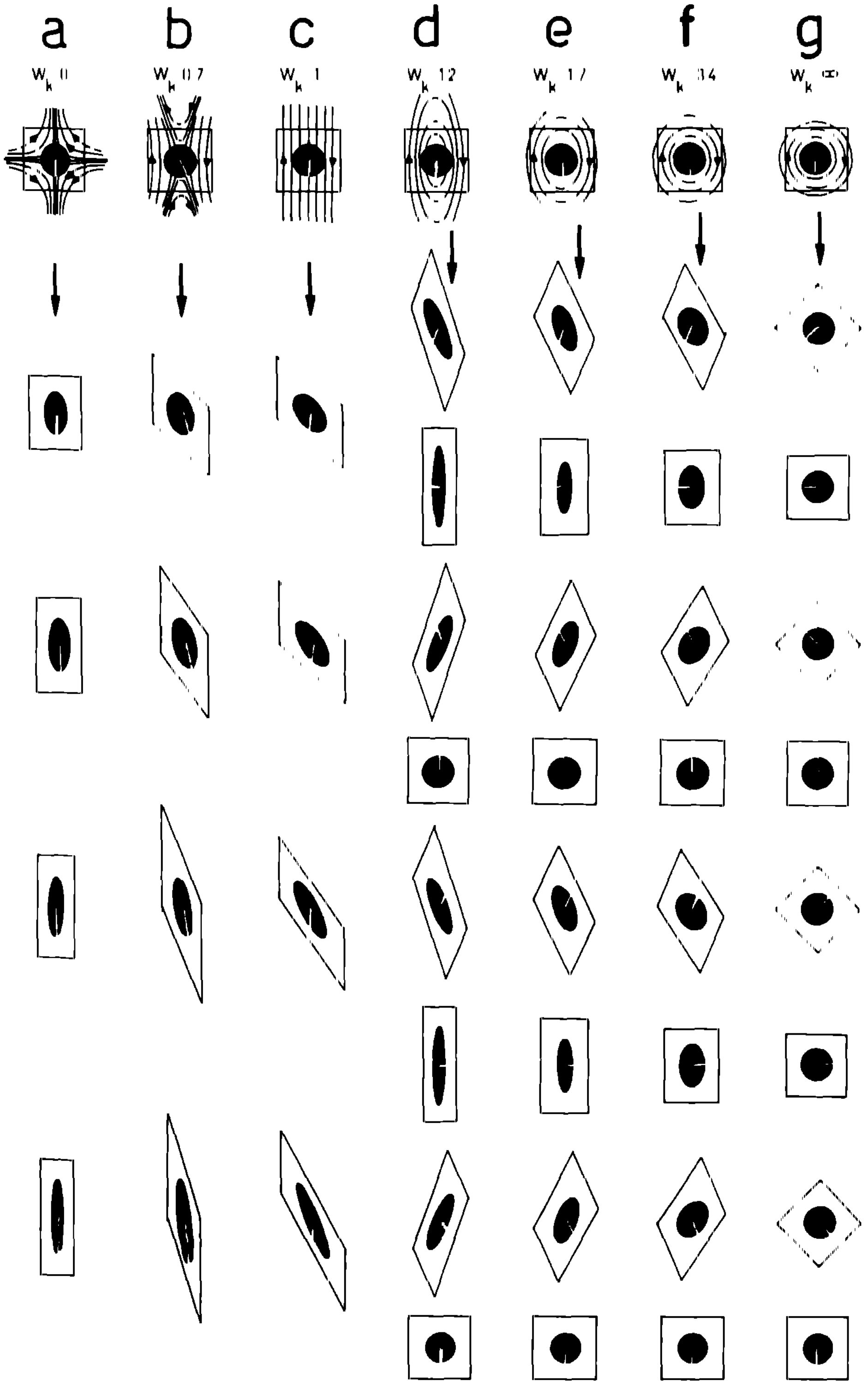

Fig. 2. Examples of homogeneous progressive plane deformation of a passive strain marker by the following particle movement paths (after Weijermars 1988b, fig. 6). (a) pure shear ($\zeta = 1$, $W_k = 0$), (b) non oscillatory flow with components of pure and simple shear superposed ($\zeta = 0.2$, $W_k = 0.7$), (c) simple shear ($\zeta = 0$, $W_k = 1$), (d) oscillatory shear ($\zeta = -0.1$, $W_k = 1.2$), (e) oscillatory shear ($\zeta = -0.3$, $W_k = 1.7$), (f) oscillatory shear ($\zeta = -0.6$, $W_k = 3.4$), and (g) rigid body rotation ($\zeta = -1$, $W_k = \infty$).

The vorticity field is given by **curl** v or the curl vector:

$$\begin{bmatrix} \dot{\omega}_x \\ \omega_y \\ \omega_z \end{bmatrix} = \mathbf{curl}\, v = \begin{bmatrix} \partial v_y/\partial z - \partial v_z/\partial y \\ \partial v_z/\partial x - \partial v_x/\partial z \\ \partial v_x/\partial y - \partial v_y/\partial x \end{bmatrix}. \qquad (6a)$$

Recall that $v_x = \partial\Psi/\partial z$, $v_y = 0$ and $v_z = -\partial\Psi/\partial x$, so that expression (6a) may be simplified into:

$$\begin{bmatrix} \dot{\omega}_x \\ \dot{\omega}_y \\ \dot{\omega}_z \end{bmatrix} = \begin{bmatrix} 0 \\ -(\partial^2\Psi/\partial x^2 + \partial^2\Psi/\partial z^2) \\ 0 \end{bmatrix}. \qquad (6b)$$

The kinematic vorticity number of expression (4b) can now be written in terms of the stream function, using (5a), (5b) and (6b):

$$W_k = \left|\frac{\partial^2\Psi/\partial z^2 + \partial^2\Psi/\partial x^2}{\partial^2\Psi/\partial z^2 - \partial^2\Psi/\partial x^2}\right| \qquad (7a)$$

with the denominator arising from $e_1 = e_{xz}$ for the particular orientation of the co-ordinate system in Fig. 1, where e_1 is always at 45° with respect to the co-ordinate axes. Substitution of the stream function of expression (3) into (7a) and differentiation reveals that W_k and ζ are related by.

$$W_k = (1 - \zeta)/(1 + \zeta). \qquad (7b)$$

Recall that special cases occur for $W_k = 0$ (pure shear strain), $W_k = 1$ (simple shear strain), and $W_k = \infty$ (rigid body rotation).

COMPUTED PARTICLE PATHS

The progressive deformation of a material volume is dictated by the particle movement paths. The stream function enables mapping of the full streamline pattern but was designed to calculate the volumetric flow rate between these streamlines and is not suitable for tracing the movement of individual particles in time. The mathematical descriptions providing the framework to track movement paths of individual particles in time are outlined in Appendix A.

It has long been customary in geological literature to refer to two basic cases of progressive deformation, pure shear and simple shear. Both of these plane deformations imply a particular assumption about the orientation of the principal stress axes with respect to a reference surface of the deforming volume (see later). Changing the orientation of the stress axes can result in progressive deformation sequences which are intermediate between pure and simple shear. A progressive deformation is fully predictable and characterized by the principal stress orientation, provided that this orientation remains constant with respect to the reference surface. It is then possible to make inferences about the time required to accomplish a particular finite deformation pattern.

Consider a specific case: a cube of viscous material resting on a solid plane, termed the reference plane in what follows. This unit volume is subjected to a stress field, and may slip freely over the reference plane relative to a single pin-axis (Fig. 3). The plane of section contains the major stress axes and coincides with the XZ-plane of a Cartesian frame of reference. The reference plane coincides with the XY-surface and the pin axis is parallel to the Y axis. The bottom of the cube is kept in tight contact with the reference plane for any orientation of the deviatoric stress field. The cube may be thought of as part of a body with infinite lateral extent in the direction of the second principal stress axis, so that deformation remains plane. Also, the cube remains incompressible in response to instantaneous stresses and long term volume changes (accompanying solution transfer and metamorphic processes in rocks) also are excluded. Consequently, deformation will be isochoric,

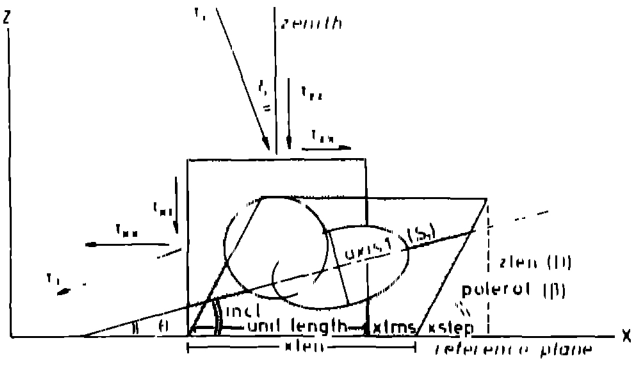

Fig. 3. Sketch section through the deforming unit volume to show definitions of the angle, ζ, of the principal deviatoric stress, t_1, with respect to the normal to the reference plane, the inclination, θ, of the major axis of the strain ellipsoid, and the principal stretch, S_1. The angles θ and ζ are measured from lines 90° apart to account for the fact that S_1 of the incremental strain ellipsoid is, by definition, always the largest stretch and thus perpendicular to t_1. The quantities incl (θ), polerot (β), xlen, xtrns, xstep, zlen (D), and axis1 (S_1) are used extensively in the computer program of Appendix B and are included here mainly for the record.

and additionally, is assumed to be homogeneous on the scale of the unit volume considered here. The assumption of homogeneous deformation implies that body forces in the unit volume are negligibly small as compared to the surface forces.

The rate of displacement ($\dot{x}_i$) of particles x_i in XYZ space can be described by the Eulerian rate of displacement equation.

$$\dot{x}_i = L_{ij}x_j \qquad (8)$$

The components of the rate of displacement tensor L_{ij} for the situation outlined in the definition sketch of Fig. 3 can be obtained as follows. Realize that the components of solid body rotation in the anti-symmetric part of L_{ij} do not alter distances between fluid particles and thus do not involve stress. The stress induces strain rates, as described by the strain rate tensor, which for the configuration of Fig. 3 is (using $\dot{e}_{zz} = -\dot{e}_{xx}$).

$$D_{ij} = \begin{bmatrix} \dot{e}_{xx} & 0 & \dot{e}_{xz} \\ 0 & 0 & 0 \\ \dot{e}_{zx} & 0 & -\dot{e}_{xx} \end{bmatrix} \qquad (9a)$$

The boundary condition of plane strain reduces the vorticity tensor to:

$$W_{ij} = \begin{bmatrix} 0 & 0 & -\dot{\omega}_y/2 \\ 0 & 0 & 0 \\ \dot{\omega}_y/2 & 0 & 0 \end{bmatrix} \qquad (9b)$$

Recall that $\dot{e}_{xz} = \dot{e}_{zx} = \frac{1}{2}[(\partial v_z/\partial x) + (\partial v_x/\partial z)]$ and $\dot{\omega}_y = [(\partial v_z/\partial x) - (\partial v_x/\partial z)]$ (Appendix A). The stable reference plane does not allow for rotation of the base of the block relative to the XYZ frame of reference, so that $\partial v_z/\partial x = 0$. This implies that, numerically, $\dot{\omega}_y/2 = -\dot{e}_{xz}$.

Consequently, the rate of displacement tensor L_{ij} can be expressed in terms of the normal and shear components of the strain rate

$$L_{ij} = \begin{bmatrix} \dot{e}_{xx} & 0 & 2\dot{e}_{xz} \\ 0 & 0 & 0 \\ 0 & 0 & -\dot{e}_{xx} \end{bmatrix} \tag{9c}$$

This is only valid for the choice of reference frame as defined in Fig 3. Note that tensor shear strain rate $\dot{e}_{xz}$ relates to the engineering shear strain rate $\dot{\gamma}_{xz}$ by $2\dot{e}_{xz} = \dot{\gamma}_{xz}$.

The position of any particle at a particular time t can be found by solving the partial differentials of the rate-of displacement equations (8) using L_{ij} as defined in expression (9c). For complex flow fields, this integration can only be solved by numerical iteration (e.g. McKenzie 1979), but analytic integration is straightforward for the simple flow and boundary conditions considered here. Methods for analytic solution of the time derivatives of the velocity field have been explained in detail by Ramberg (1975a,b), but his equations may be abbreviated considerably (see Appendix A).

Solution of equations (8) with the particular L_{ij} of expression (9c) yields the deformation tensor (using Appendix A):

$$F_{ij} = \begin{bmatrix} \exp(\dot{e}_{xx}t) & 0 & (2\dot{e}_{xz}/\dot{e}_{xx})\sinh(\dot{e}_{xx}t) \\ 0 & 1 & 0 \\ 0 & 0 & \exp(-\dot{e}_{xx}t) \end{bmatrix} \tag{10}$$

which is similar to the matrices comprised in equation (6) of Giesekus (1962), equation (38) of Ramberg (1975a) and equation (28) of McKenzie (1979)—the first and last only after a 45° transformation of the reference frame.

The normal and shear components of the strain rate tensor D_{ij} are related directly to τ_{xx} and τ_{xz}, the normal and shear components of the two-dimensional deviatoric stress tensor T_{ij} (see Appendix A, equation A5):

$$\dot{e}_{xx} = \tau_{xx}/2\eta \tag{11a}$$

$$\dot{e}_{xz} = \tau_{xz}/2\eta. \tag{11b}$$

The viscosity η in expressions (11a) and (11b) may be either Newtonian or an effective viscosity accounting for non Newtonian flow This follows from the assumption of homogeneous deformation, which implies that the deviatoric stress is constant throughout the unit volume. Since there is no spatial variation in the strain rate, the dynamic viscosity may not vary during flow. This is fulfilled if the rheology of the unit volume is Newtonian, but also for any other intrinsic rheology as each pair of stress and strain rate values plots as a single point in the log-log space of a flow diagram (e g see fig. 3 in Weijermars & Schmeling 1986) Note that I prefer using τ_{xx} for the deviatoric normal stress rather than σ_{xx}, adopting Fung's (1965) system of reserving τ for deviatoric stresses and σ for the total stresses, the indexes are sufficient to distinguish the normal and shear components

The normal and shear strain rates can now be related directly to the orientation ξ of the principal deviatoric stress τ_1 with respect to the normal to the reference plane (Fig 3), making use of the equations for the Mohr circle of stress (cf. Means 1976)

$$\tau_{xx} = \frac{\tau_1 + \tau_3}{2} + \frac{\tau_1 - \tau_3}{2}\cos 2\xi \tag{12a}$$

$$\tau_{xz} = \frac{\tau_1 - \tau_3}{2}\sin 2\xi \tag{12b}$$

For biaxial isochoric flow $\tau_1 = -\tau_3$ so that expressions (12a) and (12b) simplify to:

$$\tau_{xx} = \tau_1 \cos 2\xi \tag{13a}$$

$$\tau_{xz} = \tau_1 \sin 2\xi. \tag{13b}$$

Substitution of (13a) and (13b) into (11a) and (11b) yields:

$$\dot{e}_{xx} = (\tau_1 \cos 2\xi)/(2\eta) \tag{14a}$$

$$\dot{e}_{xz} = (\tau_1 \sin 2\xi)/(2\eta) \tag{14b}$$

It follows from expressions (14a) and (14b) that the deformation tensor F_{ij} in expression (10) is fully described if the orientation ξ and magnitude τ_1 of the principal deviatoric stress is known together with the viscosity and the time t elapsed since the onset of deformation

Consequently, the movement path of any particle (x_0, y_0, z_0) is described by the deformation tensor expression:

$$\begin{bmatrix} x \\ z \end{bmatrix} = \begin{bmatrix} A & B \\ C & D \end{bmatrix} \begin{bmatrix} x_0 \\ z_0 \end{bmatrix} \tag{15}$$

with

$$A = \exp(R_t \cos 2\xi) \tag{16a}$$

$$B = \tan 2\xi\,[\exp(R_t \cos 2\xi) - \exp(-R_t \cos 2\xi)] \tag{16b}$$

$$C = 0 \tag{16c}$$

$$D = \exp(-R_t \cos 2\xi) \tag{16d}$$

and non-dimensional time $R_t = (t\tau_1)/(2\eta)$ Note that y_0 does not change in planar flows, so that $y = y_0$ in all cases.

Expression (15) can be formulated in terms of algo

Fig 4 Computer graphic representation of streamline patterns induced by the principal deviatoric stress, τ_1 (compressive, plane strain), of particular orientations (as specified in the caption of each image and outlined by the green line) with respect to the reference plane The rheology is isotropic (anisotropy factor = 1). The direction of flow along the hyperbolic particle movement paths is away from the asymptote nearest the major principal stress axis and towards the asymptote furthest from the stress axis Flow along the asymptotes themselves is away from and towards the origin for the asymptote furthest from and nearest to the stress axis, respectively Flow fields for ξ and $\xi' = 90° - \xi$ are mirror images about the Z axis, but look different as the algorithm used to visualize them picks different, evenly spaced particles along the X axis and Z axis, for $\xi < 45°$ and $\xi \geq 45°$, respectively The images were photographed directly from the monitor and may include slight distortions arising from the curvature of the screen Similar particle paths have been visualized previously (e g Giesekus 1962, Ramberg 1975a,b, Bentley & Leal 1986), but the systematic relationship with the principal deviatoric stress axis is first outlined here

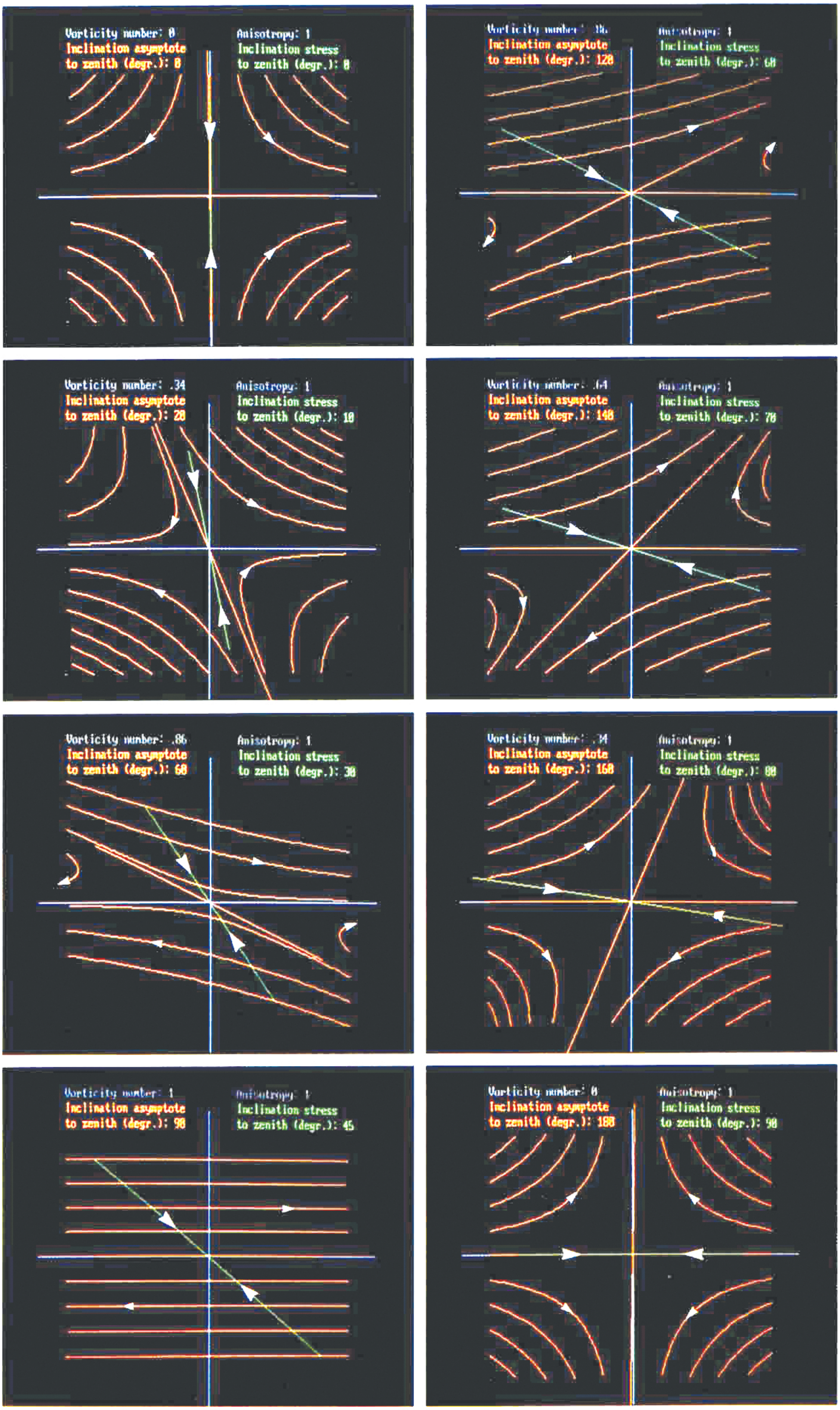
Vorticity number: 0
Inclination asymptote
to zenith (degr.): 0
Anisotropy: 1
Inclination stress
to zenith (degr.): 0
Vorticity number: .86
Inclination asymptote
to zenith (degr.): 120
Anisotropy: 1
Inclination stress
to zenith (degr.): 60
Vorticity number: .34
Inclination asymptote
to zenith (degr.): 20
Anisotropy: 1
Inclination stress
to zenith (degr.): 10
Vorticity number: .64
Inclination asymptote
to zenith (degr.): 140
Anisotropy: 1
Inclination stress
to zenith (degr.): 70
Vorticity number: .86
Inclination asymptote
to zenith (degr.): 60
Anisotropy: 1
Inclination stress
to zenith (degr.): 30
Vorticity number: .34
Inclination asymptote
to zenith (degr.): 160
Anisotropy: 1
Inclination stress
to zenith (degr.): 80
Vorticity number: 1
Inclination asymptote
to zenith (degr.): 90
Anisotropy: 1
Inclination stress
to zenith (degr.): 45
Vorticity number: 0
Inclination asymptote
to zenith (degr.): 180
Anisotropy: 1
Inclination stress
to zenith (degr.): 90

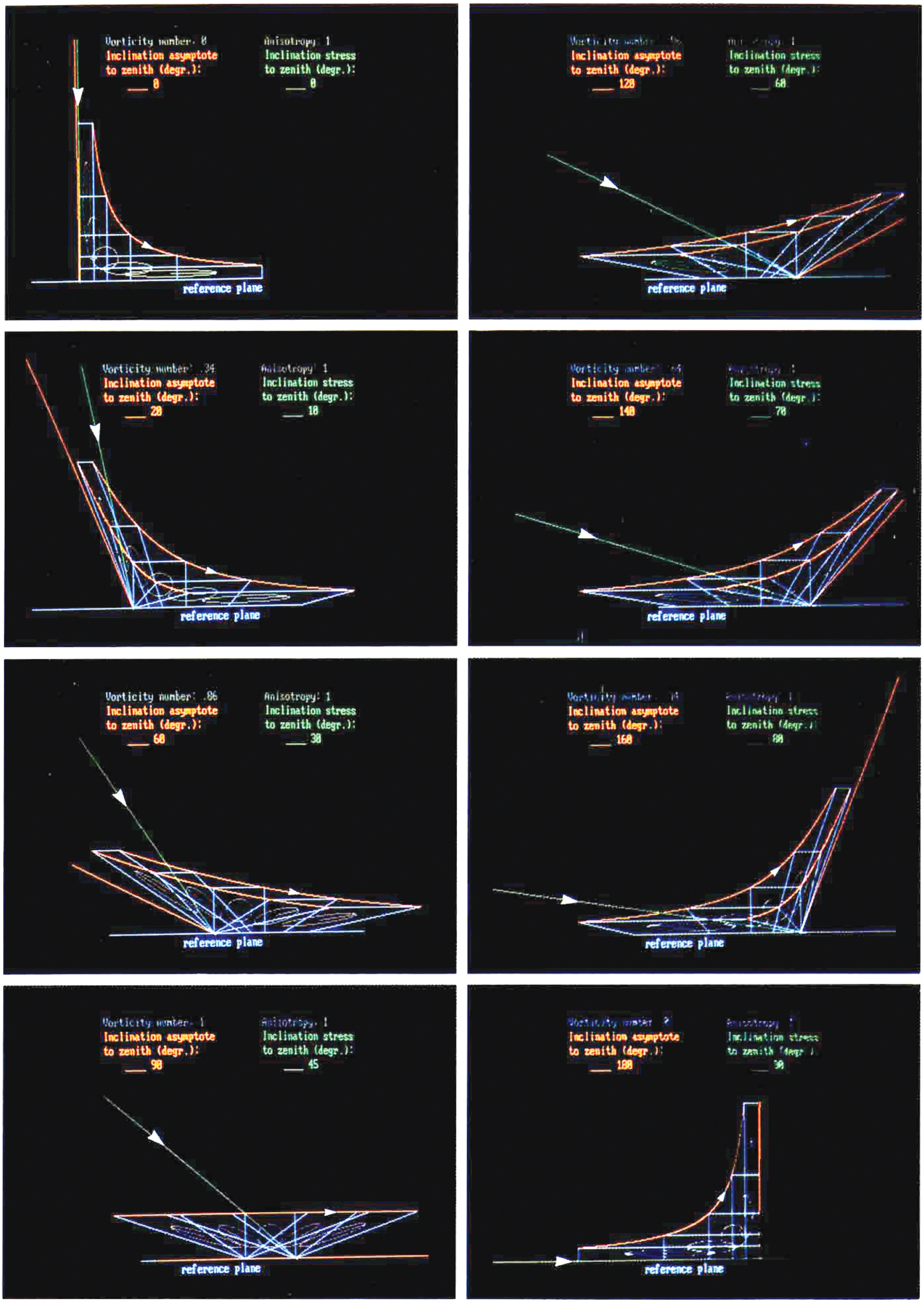
Vorticity number: 0
Anisotropy: 1
Inclination asymptote to zenith (degr.):
0
Inclination stress to zenith (degr.):
0
reference plane
Inclination asymptote to zenith (degr.):
120
Inclination stress to zenith (degr.):
60
reference plane
Vorticity number: .34
Anisotropy: 1
Inclination asymptote to zenith (degr.):
20
Inclination stress to zenith (degr.):
10
reference plane
Inclination asymptote to zenith (degr.):
140
Inclination stress to zenith (degr.):
70
reference plane
Vorticity number: .86
Anisotropy: 1
Inclination asymptote to zenith (degr.):
60
Inclination stress to zenith (degr.):
30
reference plane
Inclination asymptote to zenith (degr.):
160
Inclination stress to zenith (degr.):
80
reference plane
Vorticity number: 1
Anisotropy: 1
Inclination asymptote to zenith (degr.):
90
Inclination stress to zenith (degr.):
45
reference plane
Inclination asymptote to zenith (degr.):
180
Inclination stress to zenith (degr.):
90
reference plane

rithms and run on a PC or Laptop computer equipped with graphics to visualize the streamline patterns arising in our unit volume in response to any stress with a particular orientation ξ. Software developed by the author is discussed in Appendix B. Figure 4 illustrates several examples of two dimensional flow patterns, emphasizing the gradual change in the pattern as the inclination of the principal stress axis varies from parallelism ($\xi = 90°$) to orthogonality ($\xi = 0°$) with respect to the reference plane. The flow pattern shows the movement of particles about any point within the deforming unit volume. The horizontal axis (in blue) is parallel to the reference plane at the base of the block. Note that the streamline patterns are fixed for any particular ξ, irrespective of the magnitude of τ_1, and η, provided that $t > 0$. The anisotropy factor is unity for all streamline patterns in Fig. 4 as the material is isotropic. The effect of orthotropy has been treated elsewhere (Weijermars in preparation).

Examples of some of the flow patterns in Fig. 4 have been previously visualized in analytical studies (Ramberg 1975a,b, Ramsay & Huber 1983) and experimental studies (Fuller & Leal 1981, Bentley & Leal 1986), or both (Giesekus 1962). However, the systematic relationship of these flow patterns with the orientation of the deviatoric stress axes is outlined here for the first time.

FLOW ASYMPTOTES

The streamline patterns in Fig. 4 all possess a unique set of two straight streamlines, except for $\xi = 45°$ where they coincide. These straight streamlines—traces of the eigenvector planes—are asymptotes to the hyperbolas that form the flow patterns. One eigenvector plane is asymptotic to the exit flow, the other is asymptotic to the entrance flow. The asymptote to the exit flow coincides with the X axis for any $\xi < 45°$. The asymptote to the entrance flow coincides with the X axis for any $\xi > 45°$.

Figure 4 also specifies the kinematic vorticity number for each flow. The acute angle (α) between the X axis and the other flow asymptote is related to the kinematic vorticity number by (cf. Bobyarchick 1986).

$$W_k = \cos\alpha \tag{17a}$$

The kinematic vorticity number W_k can also be related to the orientation ξ of the principal deviatoric stress τ_1. This is because W_k can be expressed as a function of $\dot{e}_{xx}$ and $\dot{e}_{xz}$, i.e. the normal and shear components of the two dimensional strain rate tensor. The vorticity $\dot{\omega}_2$ has a magnitude equal to that of the engineering shear strain rate $-\dot{\gamma}_{xz} = -2\dot{e}_{xz}$. Substitution in expression (4b) and using expressions (14a) and (14b) yields:

$$W_k = \sin 2\xi. \tag{17b}$$

Combining expressions (17a) and (17b) and eliminating W_k yields the relationship between α and ξ:

$$\alpha = \cos^{-1}(\sin 2\xi). \tag{18a}$$

Negative angles are measured clockwise and positive angles are measured anti clockwise. Expression (18a) can be simplified by defining $\alpha' = 90° - \alpha$, so that

$$\alpha' = 2\xi \quad \text{or} \quad \alpha = 90° - 2\xi \tag{18b}$$

Expression (18b) has been used to determine the inclination of the second asymptote with respect to the normal to the reference plane for all flow patterns in Fig. 4. Note that the asymptote inclinations in Fig. 4 are specified as positive angles, i.e. measured in an anti clockwise direction with respect to the reference plane normal or zenith. The inclination of the asymptote to the hyperbolic flow paths is equal to twice the angle of inclination of the deviatoric stress.

FINITE DEFORMATION PATTERNS

A deformation may be termed progressive if the observer is able to examine a continuous sequence of configurations through which a body passes, unlike the general term 'deformation' which refers to the difference in geometry of two distinct finite states of a body (Flinn 1962). The particle paths computed and illustrated in Fig. 4 allow reconstruction of the progressive deformation of material volumes.

Again, consider the deformation tensor of expression (15) with the terms A, B, C and D as specified in expressions (16a)-(16d). The principal axes of the strain ellipsoid at any time t can be characterized in terms of eigenvalues of the deformation tensor, S_1 and S_3, using the principal quadratic elongations λ_1 and λ_3. The latter—themselves eigenvalues of the strain ellipse expression in matrix form (Ramberg 1975a, p. 30)—can be calculated from the deformation tensor components A, B, C and D, using the following algorithms:

$$\lambda_1 = 0.5[(K) + \sqrt{[(K^2) - 4(AD - BC)^2]}] \tag{19a}$$

$$\lambda_3 = 0.5[(K) - \sqrt{[(K^2) - 4(AD - BC)^2]}] \tag{19b}$$

with $K = A^2 + B^2 + C^2 + D^2$. For example, a unit sim

Fig. 5. Computer graphic representation of progressive deformation of a unit volume of rock in ductile creep and plane strain due to stress fields oriented as in Fig. 4. The images are non-dimensional. The increments of finite strain are 2 Ma apart for a rock with isotropic viscosity of 10^{21} Pa s deformed by a deviatoric stress of 20 MPa. This corresponds to a strain rate of 10^{-14} s^{-1}. The time scale can be adapted to other situations applying the scaling rules of expressions (23a) and (23b). The two hyperbolic flowlines (in red) show the movement of particles in the upper left and upper right hand corners of the deforming volume, relative to the pin point at the intersection of the stress axis (in green) and the reference plane (in blue). The full flow pattern around any particle above the reference plane is given in Fig. 4. The orientation of the axis of largest stretch of the strain ellipsoid at infinitely large strain is indicated by the inclination of the asymptote (in red). Positive angles are measured anti-clockwise. The images were photographed directly from the monitor and are not corrected for the curvature of the screen. The character of the images was inspired by Ramberg's (1975a) fig. 3, but again, the systematic dependence of the progressive deformation on the stress orientation is first emphasized here.

ple shear which has $(A, B, C, D) = (1,1,0,1)$ gives $\lambda_1 = 2.62$. Expressions (19a) and (19b) were adopted from Ramsay & Huber (1983, appendix B, equation B 19, p. 287) and are also implied in Thompson & Tait (1879) and Jaeger (1956). The length of the major and minor axes of the strain ellipsoid can be expressed in terms of the stretches S_1 and S_3

$$S_1 = 1 + e_1 = \sqrt{\lambda_1} \tag{20a}$$

$$S_3 = 1 + e_3 = \sqrt{\lambda_3} \tag{20b}$$

and the axial ratio $R = \sqrt{(\lambda_1/\lambda_3)}$. Note that S_1 and S_3 can also be obtained directly from $R = S_1/S_3$ and the boundary condition of plane isochoric strain so that $S_1 \cdot S_3 = 1$. Consequently, the ellipticity may be written as $R = (S_1)^2 = \lambda_1$. The condition of plane strain implies that the intermediate axis of the strain ellipsoid, S_2, remains unchanged so that $S_2 = 1$.

The angle θ between the major axis of the finite strain ellipsoid and the X axis can be calculated for any time t, from the expression (cf. Ramsay & Huber 1983, equation B.14; also implied in Thompson & Tait 1879 and Jaeger 1956):

$$\theta = 0.5 \arctan [(2AC + 2BD)/(A^2 + B^2 - C^2 - D^2)]. \tag{21}$$

Recall that the rotation of the major axes of the strain ellipsoid is not the same as the rotation of particular material lines.

The horizontal and vertical dimensions of our deformed, initially cubic, unit volume are equal to A and D, respectively. Any initially vertical marker line within the cube is, after deformation, inclined at angle β with respect to the reference plane.

$$\beta = \arctan (D/B) \tag{22}$$

The algorithms above allow the computation of any parameter relevant to the progressive deformation history of a unit volume. A computer program can be written for calculating these parameters and displaying stages in the evolution of finite strain pertinent to a particular deformation sequence (Appendix B).

Figure 5 visualizes the progressive deformation of a unit cube for various orientations of the principal stress axis. The base of the cube is pinned at one corner and slips freely over the reference plane. The pin-line is perpendicular to the plane of section of Fig. 5 and is visible as a pin point in the lower left hand corner for $0° \leq \xi \leq 45°$ and in the lower right-hand corner for $45° \leq \xi \leq 90°$. The unit cube of this particular example comprises a rock of viscosity 10^{21} Pa s, deformed by a deviatoric stress of 20 MPa. This corresponds to a typical geological strain rate of 10^{-14} s^{-1}. The stages shown in Fig. 5 are 2 Ma apart. Stages of reciprocal deformation are included in Fig. 5 to emphasize that the patterns for similar W_k, occurring at ξ and $\xi' = (90° - \xi)$, look similar, but differ in the sense of reciprocal and progressive deformation.

Figure 6 illustrates the progressive deformation of a cubic block in a plane stress field for various values of ξ,

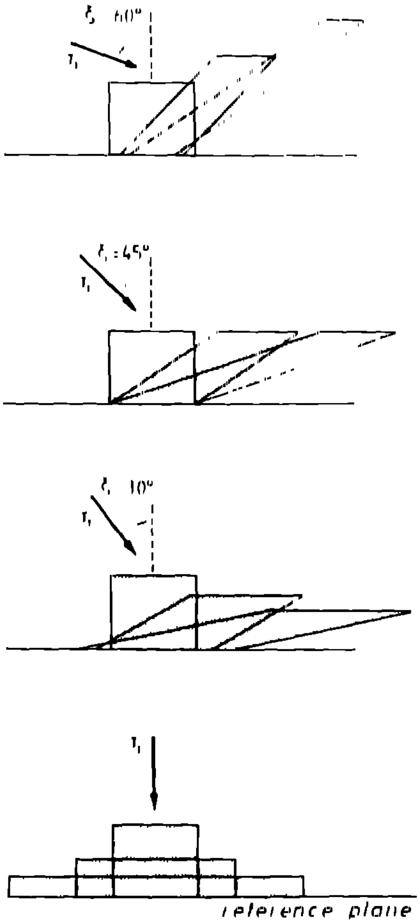

Fig. 6. Progressive deformation of a cubic block viewed perpendicular to the pin line bisecting the bottom plane. Thus the block is in two equal parts each slipping without friction over the reference plane in opposite directions. Cases given by ξ values of 0°, 30°, 45° and 60° are illustrated. Increments of finite strain are 2 Ma apart for a rock of isotropic rheology deforming at a strain rate of 10^{-14} s^{-1}. The intent is to emphasize the thickening vs thinning of the layer (of which the cube is part) resting on the reference plane, for cases of $\xi > 45°$ and $\xi < 45°$, respectively. Expression (23b) can be used for translation to other rheologies and stress fields.

with the pin line bisecting the bottom surface in two equal, rectangular areas that may slip freely over the reference plane. Increments of finite strain are similar to those shown for the same value of ξ in Fig. 5, but the pin-line is now positioned so that the macroscopic flow field includes all the flowlines illustrated above the X axis in Fig. 4 for the corresponding ξ.

The relationship between W_k, ξ and α (or $\alpha' = 90° - \alpha$) has been graphed in Fig. 7 according to expression (17b). Note that flow patterns in Fig. 4 are the same for ξ and $\xi' = 90° - \xi$ except for a rigid body rotation of 180° about the Z axis. However, the direction of flow is not the same, so that the mode of progressive deformation will be different. Comparison of the results in Fig. 5 reveals that angles ξ for σ_1-orientations larger and smaller than 45° give the same W_k, but involve different progressive deformations leading to layer thickening and thinning, respectively. Layer thinning and thickening is also visible in Fig. 6. Figure 7 therefore emphasizes that the kinematic vorticity numbers for ξ and $\xi' = 90° - \xi$ are identical, despite differences in the

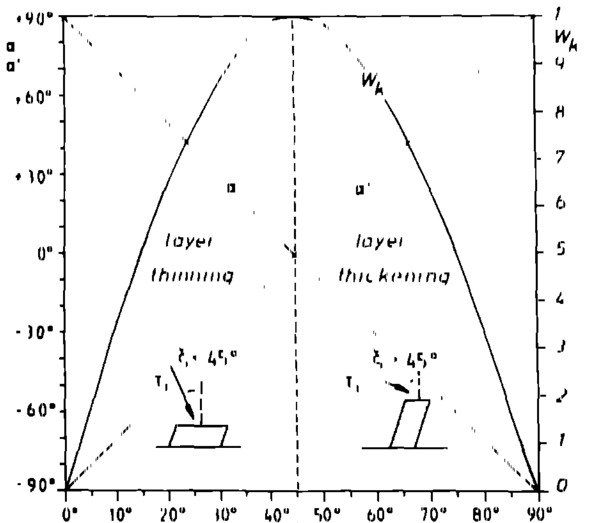

Fig. 7 Relationship between the kinematic vorticity number W_k and the angle ξ between the major principal stress axis and the normal to a reference plane The angles a and $a' = 90° - a$ between the two asymptotes of the flowline patterns for a particular ξ value are also graphed

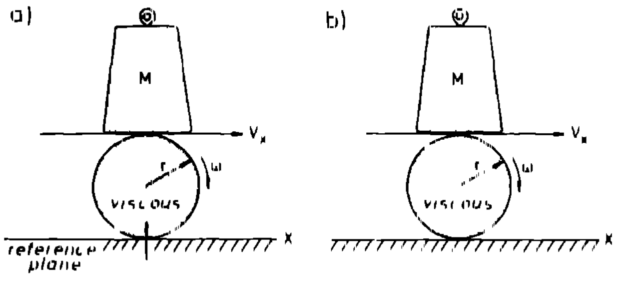

Fig 8 Sketches of an experimental set up for simulating (a) non oscillatory (i e $0 \le W_k \le 1$) and (b) oscillatory (i.e $1 < W_k \le \infty$) deformations A cylinder of radius r is rolled between a stable reference plane and a movable top plate loaded with a mass M The velocity of the top plate is v_x The cylinder in (a) is pinned to the reference plane, thus limiting the amount of rotation The cylinder in (b) may rotate freely between the two planar surfaces

progressive deformation. Consequently, the stress orientation is a unique measure for the mode of progressive deformation—the kinematic vorticity number is not

The time increments of Figs. 5 and 6 can be translated to other time scales using the following scaling rule (combining equations 12c and 12f of Weijermars & Schmeling 1986):

$$t_{new} = [(\eta_{new}\tau_{old})/(\eta_{old}\tau_{new})]t_{old} \quad (23a)$$

or

$$t_{new} = (\dot{e}_{old}/\dot{e}_{new})t_{old} \quad (23b)$$

The time scale t_{old} of Figs 5 and 6 can be converted to new time scales t_{new} by substituting into expression (23a) the following values: kinematic viscosity $\eta_{old} = 10^{21}$ Pa s, deviatoric stress $\tau_{old} = 20$ MPa, and τ_{new} and η_{new} of the new deformation sequence.

Alternatively, the time scales of Figs. 5 and 6 (and 9 and 10, see later) can be non dimensionalized (R_t) according to the following expression:

$$R_t = (t_{old}\tau_{old})/2\eta_{old} \quad (24a)$$

or

$$R_t = t_{old}\dot{e}_{old}. \quad (24b)$$

For example, the non dimensional time for the 1 Ma isochron in Fig 10 is $R_t = 0.315$

OSCILLATORY VS MONOTONIC STRAINS

Figures 4 and 5 and the associated theory comprise the entire spectrum of stress orientations possible in two dimensional, homogeneous, steady-state flows. A peculiarity of this spectrum is that streamline patterns characteristic of oscillatory strains cannot be generated by the model of Fig. 3. The relationship between the kinematic vorticity number and the stress orientation given in expression (17b) explains why monotonic and not oscillatory strains occur. It appears that W_k varies only between 0 and 1 for any particular orientation of the stress field; no oscillatory strains occur in this range (Fig 7).

Oscillatory deformation histories occur if $W_k > 1$ and Appendix A outlines why the deformation tensor is different from that obtained here if complex eigenvalues are involved in the solution of the integration of the rate of displacement equations Pfiffner & Ramsay (1982) correctly pointed out that only flow paths leading to deformations lying between pure shear and simple shear are geologically relevant for tectonic processes on a regional scale Ramberg (1975a, p. 34) explained that oscillatory strains may occur only within competent inclusions enclosed in a softer matrix The rate of strain of the inclusion must be less than that in the matrix to enhance the vorticity. This condition is only met on a small scale, unless applicable to batholiths separated by supracrustals The concept may be clarified using a mechanical analog, where the strain rate and vorticity are caused by two separate mechanical components.

Figures 8(a) & (b) show the principle schematically. A pair of initially circular cylinders, both consisting of the same viscous material and deforming by plane strain, rests on a stable reference plane, with the cylinder-axis perpendicular to the plane of flow (and view). The top of both cylinders is in contact with a plate of negligible weight. Vorticity may be given to either cylinder by pulling the top plate horizontally with velocity v_x perpendicular to the cylinder axis. A principal strain rate may be added by loading the top plates with a mass M as indicated in Fig 8 Body forces inside the cylinders are negligible in comparison to the surface forces

The systems of Figs. 8(a) & (b) differ in only one respect—the boundary condition The magnitude of the vorticity in Fig 8(a) is limited by fixing the base of the cylinder to the reference plane The top of the cylinder may roll in response to a force pulling the top plate at rate v_x, without allowing any slip at their contact. Progressive simple shear will occur if the surface load is zero ($M = 0$) and $v_x \neq 0$. Pure shear flow occurs if $v_x = 0$ and $M \neq 0$. Consequently, the configuration of Fig. 8(a) allows only for the occurrence of non oscillatory deformation histories.

Table 1. Comparison of inclination θ of the strain ellipsoid for various stretches S_1 in simple shear ($\xi \rightarrow 45°$) using equations (16a)–(16d) and (26a)–(26d). Equations (26a)–(26d) are a good approximation up to stretches of about 3. Time steps in millions of years are for strain rate 10^{-14} s^{-1}

Time (Ma)	S_1	θ (equations 16a–16d) (°)	θ (equations 26a–26d) (°)
1	1.36	36.27	36.45
2	1.81	28.84	29.65
3	2.32	23.28	24.95
4	2.87	19.19	21.73
5	3.44	16.19	19.49
6	4.03	13.92	17.82
7	4.63	12.18	16.55
8	5.23	10.81	15.57
9	5.84	9.70	14.76
10	6.46	8.79	14.10

In contrast, the magnitude of the vorticity in Fig. 8(b) is unlimited because the cylinder can roll freely, but without slip, between the reference plane and the top plate. Perfect rigid-body rotation will occur if the surface load is zero ($M = 0$) and $v_x > 0$. Again, pure shear flow occurs if $v_x = 0$ and $M > 0$, but $W_k > 1$ for any other combination of M and v_x. This is because v_x cannot effectively transfer shear stresses to the surface of the cylinder due to the boundary condition of free rotation. Consequently, the experimental configuration of Fig. 8(b) allows the modelling of oscillatory deformations.

An experiment of oscillatory deformation may be provisionally simulated by moulding a cylinder out of a high viscosity material such as PDMS (viscosity 5×10^4 Pa s, see Weijermars 1986). This viscous cylinder is then loaded by a copy of this journal and subjected to vorticity by rolling the cylinder between your desk and the journal. The distance between the journal and the table will periodically decrease and increase if you pull the journal at a slow, constant speed parallel to the table. The cylinder itself will deform in an oscillatory fashion by approximately plane strain if the cylinder axis is long relative to its radius.

STRESS FIELDS

Figure 5 suggests that, for any particular orientation of the principal deviatoric stress, the magnitude of the finite strain evolves coevally with a particular amount of finite rotation in a fashion dictated by the particle movement paths. The relationship between the magnitude of the stretch and the progressive rotation of the principal axis of finite strain has previously been established for the special case of simple shear, i.e. $\xi = 45°$ (Ramsay 1967, p. 85 ff) and other cases are implied in Ramsay & Huber (1983, session 12). It is useful to investigate the relationship between the principal stretch and rotation for any orientation of the principal stress.

The unique relationship between the principal stretch S_1, strain ellipsoid inclination θ and inclination ξ of the principal deviatoric stress, can be demonstrated by straightforward mathematics. Equation (21) expressed θ in terms of the deformation matrix components A, B, C and D. These components, as specified in expressions (16a)–(16d), can be rewritten in terms of S_1 and ξ. This is because the non dimensional time R_t used in expressions (16a)–(16d) is, in fact, also a measure of the finite strain:

$$R_t = (t\tau_1)/(2\eta) = t\dot{e}_1 = \ln S_1 \qquad (25)$$

Substitution of expression (25) into expressions (16a)–(16d) yields:

$$A = S_1^{\cos 2\xi} \qquad (26a)$$

$$B = \tan 2\xi (S_1^{\cos 2\xi} - S_1^{-\cos 2\xi}) \qquad (26b)$$

$$C = 0 \qquad (26c)$$

$$D = S_1^{-\cos 2\xi} \qquad (26d)$$

It is now obvious that equation (21) together with expressions (26a)–(26d) describe the unique relationship between ξ, S_1 and θ. Note that expression (26b) is undefined for $\xi = 45°$, but this can be circumvented by taking any ξ very close to this particular angle. Equations (26a)–(26d) are only strictly valid for pure shear (i.e. $\xi = 0°$ or $\xi = 90°$), because in other cases the approximation of R_t by $\ln S_1$ in equation (25) becomes inaccurate due to the mismatch between the incremental and finite strain ellipsoids in non-coaxial deformations. The largest mismatch occurs for simple shear ($\xi \rightarrow 45°$), but Table 1 shows that equations (26a)–(26d) still are a good approximation of the exact solutions of equations (16a)–(16d) for stretches smaller than 3.

Figure 9 graphs the relationship between the inclination angle, θ, of the strain ellipsoid major axis (with respect to the reference plane) and the magnitude of the major stretch S_1 for a family of ξs (using equations 16a–16d). Note that the principal axes of the ellipsoids for stress and incremental strain (or strain rate) coincide so that $\theta = \xi$ at the onset of the deformation. Recall that θ and ξ have been defined 90° apart (Fig. 3) to account for the fact that S_1 of the instantaneous or incremental strain ellipsoid is always perpendicular to τ_1. The subsequent evolution of finite strain and rotation of the strain ellipse is outlined by the subhorizontal curves in Fig. 9.

The plot of Fig. 9 is non dimensional, except for the isochrons. These are scaled for the particular case of rock with an isotropic viscosity of 10^{21} Pa s, deforming by a deviatoric stress of 20 MPa at a strain rate of 10^{-14} s^{-1}. The isochrons are included in Fig. 9 to demonstrate that pure shear is much more effective than simple shear for achieving large strains for a given deviatoric stress. This applies only to isotropic rheologies; the reverse holds for orthotropic viscosities where the plane of weakness lies in the shear direction (Weijermars in preparation). The difference between the finite strains achieved in pure shear and simple shear increases as the deformation progresses (Fig. 9). The isochrons in Fig. 9 can be translated to other time scales using the scaling rule of expression (23).

Figure 10 shows an alternative graph plotting the change in orthogonal thickness of a deforming layer

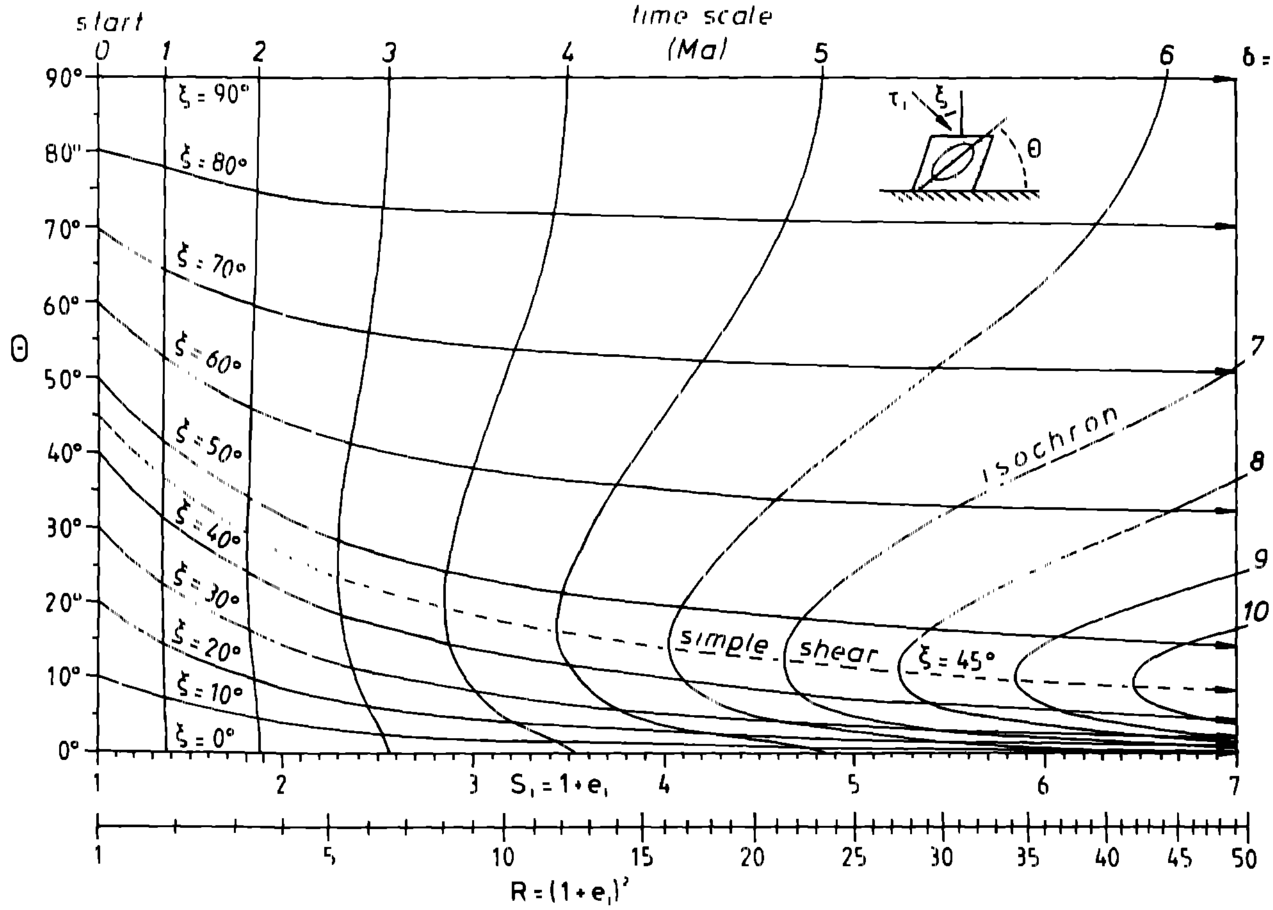

Fig. 9. Nomogram showing the relationship between the angle, θ, of the major axis of the finite strain ellipsoid with respect to a reference plane and the magnitude of the stretch, S_1, and ellipticity, R, caused by principal deviatoric stress, τ_1, inclined at 0°, 10°, 20°, 30°, 40°, 45°, 50°, 60°, 70°, 80° and 90°. The isochrons indicated refer to a rock of isotropic viscosity deforming at a strain rate of $10^{-14}\ s^{-1}$. Non dimensionalization by expression (24b) yields dimensionless times R_t = 0.315 for 1 Ma, R_t = 0.630 for 2 Ma, R_t = 0.945 for 3 Ma and R_t = 0.315x for x Ma. See also the definition sketch of Fig. 3 and expressions (20) and (21).

versus the rotation of a marker line initially perpendicular to the layer, for a variety of orientations, ξ, of the principal stress axis. Layer thickening occurs for $\xi > 45°$ and thinning for $\xi < 45°$, whilst thickness remains unchanged in simple shear ($\xi = 45°$). Layer thinning is fastest for pure shear at $\xi = 0°$, and fastest thickening occurs by pure shear at $\xi = 90°$. Note that the asymmetric 'bulge' in the isochron pattern indicates that the rotation of the initial normal is fastest for simple shear ($\xi = 45°$) at the onset of deformation, but occurs faster for smaller values of ξ if the deformation progresses.

DETERMINATION OF PALAEOSTRESS

Ductile deformation patterns caused by solid state creep in rocks are limited to very low Reynolds number flows so that inertia effects may be neglected (e.g. Weijermars & Schmeling 1986). This means that deformation ceases instantaneously as soon as the driving force stops. It is therefore potentially possible to recover the orientation of palaeostress axes responsible for natural deformation patterns from field measurements of their finite strain and rotation components, after confirming that there has been flow at a constant stress orientation (expressions 21 and 26a–26d). Methods to recover the strain from natural flow markers are available and require only knowledge of the initial geometries (of fossils, pairs of lines, imbricated pebbles, etc.; cf. Ramsay & Huber 1983, Lisle 1988). However, the component of finite rotation can only be quantified if the initial orientation of such flow markers is known.

At this point it seems appropriate to quote what has been termed a general theorem (Hobbs *et al.* 1976, p. 31): "Any homogeneous constant volume deformation can be expressed as a pure shear together with a rigid body rotation and a rigid body translation". This theorem is commonly used to discourage geologists from attempting to determine whether a particular deformation pattern in the field has been formed by pure or simple shear. "The only differences between such a pure shear and a simple shear are a rigid body rotation and a rigid body translation" (Hobbs *et al.* 1976, p. 32).

Perhaps the difficulty of distinguishing between rotational and non rotational deformation histories has been over emphasized in the past. It has overlooked situations where ductile rock has flowed adjacent to relatively rigid walls. A unit volume of rock with one face adjacent to a stable rigid boundary will be unable to rotate that contact if strain compatibility rules are res-

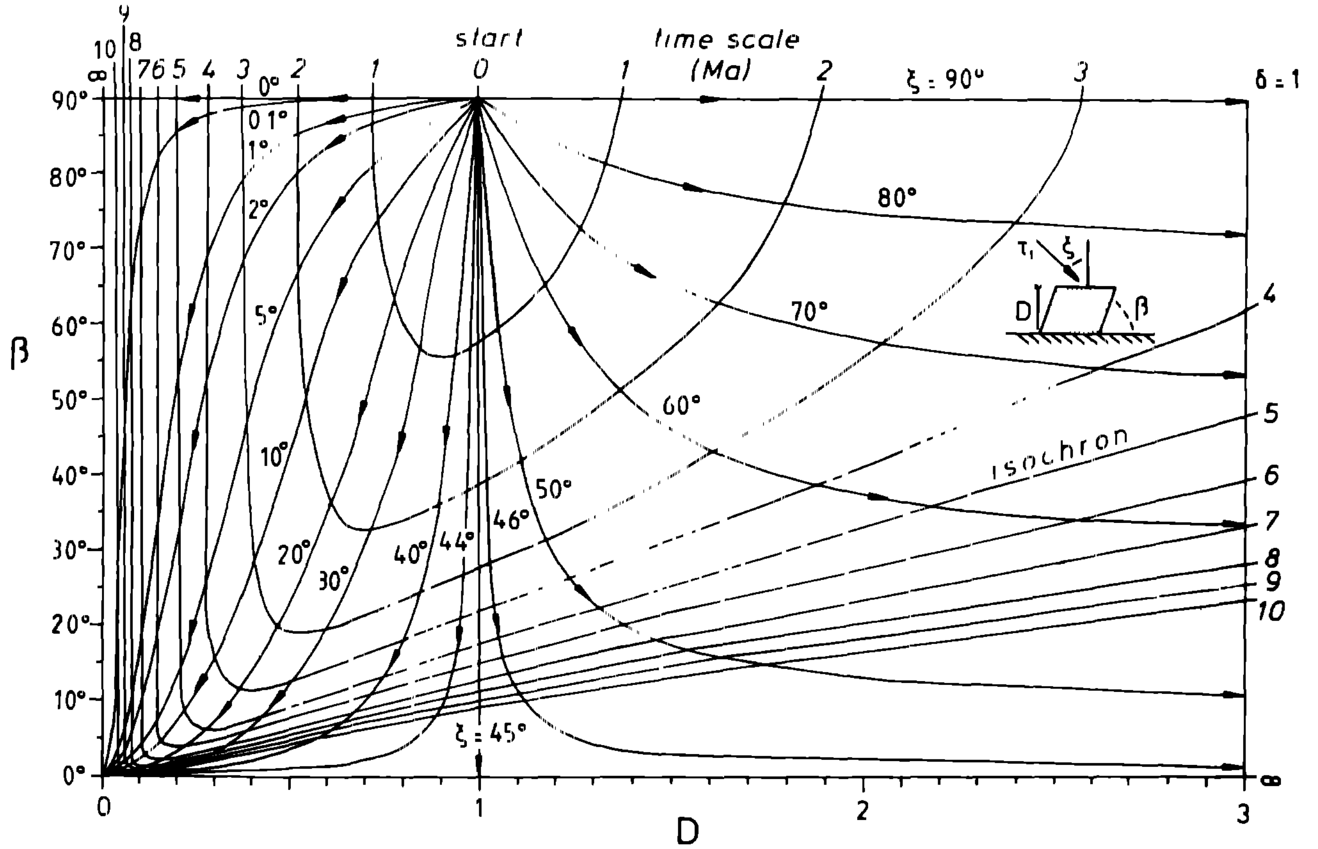

Fig. 10. Nomogram showing the relationship between the change in layer thickness (expressed as stretch D) and the rotation (β) of a line initially orthogonal to the reference plane for various orientations, ξ, of the principal deviatoric stress. The angle β is 90° at time 0, when deformation begins. The vertical line for ξ = 45° shows that there is no change in layer thickness for simple shear. The field to the left shows how layer thinning occurs if ξ is larger than 45°. Note that, in pure shear, layer thinning or thickening does not involve a change in β, and therefore pure shear plots along the top line of the diagram. See also the definition sketch of Fig. 3 and expression (22).

pected. There are many situations in nature where this boundary condition may have been maintained during the deformation. For example, ductile shear zones below fold nappes, orogenic belts adjacent to cratons and segments of lithospheric extension may all comprise ductilely deformed structures, at particular depths, deforming between relatively rigid walls. The stretch of the bulk strain ellipsoid and its inclination with respect to those walls provides a potential measure of rotation which can be plotted in Fig. 9 to determine ξ. Alternatively, the rotation and change in length of a marker line initially orthogonal to the rigid walls of the deformed zone can be used to determine ξ from the plot of Fig. 10.

Example

The graph of Fig. 9 can be used to plot pairs of (R,θ) or (S_1,θ) measured in the field. If the deformation markers used were truly passive and have a good strain memory, these pairs cluster on the plot of Fig. 9 and thus provide an estimate for ξ. In order to avoid discussions on the reliability of the strain memory of deformation patterns in natural rocks, I resort to a laboratory experiment. Figure 11 shows sketches of John Ramsay and Martin Huber on the side of a Plasticene block of high viscosity deformed by a stress of consistent, but unknown orientation. Plasticene has a perfect strain memory and is unable to recover. The base of the block was lubricated with a low viscosity oil allowing free slip over a stable reference plane relative to an arbitrary pinline. The block was further confined between two plexiglass walls so that deformation remained planar. The images of both Ramsay and Huber were nicely round in undis-

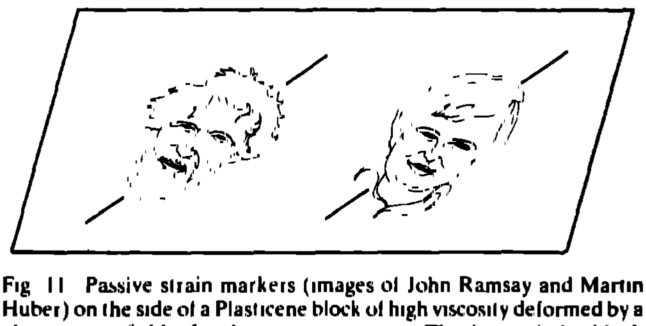

Fig. 11. Passive strain markers (images of John Ramsay and Martin Huber) on the side of a Plasticene block of high viscosity deformed by a plane stress field of unknown orientation. The base of the block remained stable throughout the deformation. The finite stretch S_1 = 1.14 and the inclination of the greatest axis of the strain ellipsoid with respect to the base of the deformed block is θ = 36°. These data are sufficient to infer from the nomogram of Fig. 9 that the major axis of stress causing the deformation was oriented at 40° to the normal to the base of the block. The same inclination of the stress axis can be determined, using Fig. 10, from the fractional change in orthogonal thickness of 0.96 and the rotation of the edge of the block, which was initially at 90° to the reference plane, and is now at 75°.

torted mode, and show no area change in the deformed state

This allows determination to be made of the finite strain and inclination of the strain ellipsoid axes with respect to the base of the deformed block. The ellipticity of both faces is $R = 1.3$ (corresponding to a stretch $S_1 = \sqrt{1.3} = 1.14$) and their inclination angle is 36°. This finds a ξ value of 40° in Fig. 9. The alternative method employs the fractional change in height of the block of 0.96 and the rotation of the vertical edge of the block from 90° to 75°. Plotting these data in Fig. 10 also yields a ξ value of 40°. This means that the Plasticene block of Fig. 11 must have been deformed by a stress field with its major principal axis at 40° to the normal of the reference plane, i.e. the base of the Plasticene block.

DISCUSSION

The theory developed here concerns deformation patterns formed (1) in plane strain; (2) at steady state, (3) without volume change, and (4) adjacent to a rigid boundary. The feasibility of these assumptions will be discussed below.

(1) In two dimensional flows, all displacement occurs in the plane of flow, and there are no velocity components perpendicular to this plane. This condition is likely to apply to fold belts, shear zones, nappe complexes and diapiric ridges. Three dimensional flow fields, involving significant deviation from plane strain, are responsible for the emplacement of granite batholiths, mantled gneiss domes and salt stocks. Progressive deformation in three dimensional flows has been analysed by Ramberg (1975b).

(2) Steady state is assumed, *but the magnitude of the stress and the consequent flow rate need not remain constant*. Steady state is assumed here in the sense that the deviatoric stress remains at a constant angle with respect to the reference plane. In geological flows for which condition (1) of plane strain applies, the major and minor axes of deviatoric stress will lie in the plane of straining. Whether the stress axes rotate within the plane of deformation depends upon the nature of the forces that drive the deformation. Most geological flows are in some way or other due to lithospheric plate driving mechanisms. Reorientation of the regional stress axes on the time scale of tectonic episodes, say 10 Ma, is less likely to occur in view of the slow rate at which convective forces reorganize (e.g. see references in Weijermars 1988a). There remains the possibility that the reference plane will rotate, even in stable stress fields. Nonetheless, there are many situations in nature where rock is deforming in a ductile fashion adjacent to relatively rigid walls.

(3) The deforming block is assumed to remain incompressible in response to instantaneous stresses. This usually holds for rocks deforming at crustal depths where ductile creep may occur, as any pore space will be closed due to the high confining pressures prevailing at such depths (say >7 km). The long-term volume changes which may be caused by solution transfer and metamorphic processes in some rocks also are excluded. Note that the present theory will still hold if the volume change is equal in all directions. This may be so in metamorphic volume change, but is certainly unlikely in solution transfer. The error introduced by applying the present theory to rocks affected by such volume changes is difficult to predict.

The estimation of palaeostress axes from strain measurements in natural rocks also is sensitive to the strain memory of the particular rock. Strain memories may be erased by static recrystallization or annealing. This is most likely in rocks which resided for a long time at deep crustal levels after deformation. Annealing is least likely to occur in rock brought relatively quickly to our vision by isostatic recovery and continuous erosion of the surface. The critical time scale for such annealing to occur will vary with rock type and has not yet been studied in sufficient detail to allow quantitative estimates.

(4) The boundary condition assumed in the present analysis is that the deforming volume may slip freely over the stable wall rock relative to a fixed point (the boundary is a fault). In nature, the degree of slip at rock interfaces is controlled by a range of physical parameters. These include confining pressure, water pressure, fracture density and ambient temperature. Byerlee's law in crustal strength profiles suggests that solid state slip by frictional glide will generally not occur at depths where rock may deform in a ductile fashion (e.g. Goetze & Evans 1979). The free slip condition therefore will be most nearly fulfilled in geological settings where the rock volume deforming in ductile flow is separated from relatively rigid wall rock by a thin zone of low viscosity rock. Bird (1984) has provided experimental support for the idea that major fault zones, weathered by hydrothermal circulation, may have extremely low frictional resistance. In such cases the interface may behave as a stretching fault (Means 1989, 1990). If slip is constrained, strain compatibility problems will limit the mode of deformation to simple shear with various amounts of volume change as discussed in detail by Ramsay & Graham (1970) (cf. Ramsay & Huber 1983, p. 47, 1987).

CONCLUSIONS

Palaeostress magnitude may be recovered from grain size studies of quartz fabrics (cf. Etheridge & Wilkie 1981). A complementary method for special conditions, first outlined here, now also allows potential recovery of the orientation of the principal axes of palaeostress. Knowledge of the flow field provides a sound basis for discussing the significance of the kinematic vorticity number, various modes of progressive deformation and how these are controlled by the stress orientation.

The deformation tensor, obtained by solving differential equations connected with the rate of displacement or velocity gradient tensor, is expressed in time dependent terms comprising only the normal and shear components of the strain rate tensor (expression 10) Mohr's equations of stress can be used to link the strain rates to the major principal stress This derivation yields a time-dependent deformation tensor which is expressed in terms of the dynamic viscosity and major deviatoric stress (magnitude and orientation with respect to a reference plane), (expressions 15 and 16a-16d)

The deformation tensor can be non dimensionalized by rewriting its components in terms only of the orientation, ξ, of the major axis of deviatoric stress, the stretch, S_1, and rotation component, θ, of deformation (expression 26a-26d). Estimates of the rotation and stretch of finite strain ellipsoids in nature are sufficient to identify the orientation of the axes of palaeostress from a nomogram first introduced here (Fig. 9) Alternatively, the direction of palaeostress axes can be determined from the rotation and change in length of a marker line initially normal to the reference plane (Fig. 10)

Finally, the theory developed here should be applied with care. Although fields of inhomogeneous deformation may be partitioned into smaller domains of approximately homogeneous deformation (Cobbold 1977, 1979, 1980, Cobbold & Percevault 1983, Cutler & Cobbold 1985), such domains will continuously be reorientated with respect to the principal stress directions. In such cases, recovery of the palaeostress trajectories could still be possible by first reconstructing the flow lines leading to the particular pattern of inhomogeneous deformation concerned

Acknowledgements—The idea of this paper was born during a refresher course in structural geology taught by the author to senior field geologists at the Geological Survey of Sweden (Uppsala, May 1989) "How can we recover the orientation of the tectonic stress field", was one of those questions which kept recurring This particular question, which has survived several generations of geologists and decades of much criticized speculation, indeed lies at the heart of many tectonic problems This manuscript matured by penetrative discussions with Win Means, Hans Ramberg and John Ramsay, and critical editorial guidance by Peter Hudleston and Chris Talbot Programming, draftwork and photographs were all done by the author This study has been performed whilst holding a post doctoral travel grant from the Swedish Natural Science Research Council

REFERENCES

Bentley, B J & Leal, L G 1986 A computer controlled four roll mill for investigations of particle and drop dynamics in two dimensional linear shear flows. *J Fluid Mech* **167**, 219–240

Bird, P 1984 Hydration phase diagrams and friction of montmorillonite under laboratory and geological conditions, with implications for shale compaction, slope instability, and strength of fault gouge *Tectonophysics* **107**, 235–260.

Bobyarchick, A R 1986 The eigenvalues of steady flow in Mohr space *Tectonophysics* **122**, 35–51.

Cobbold, P R 1977 Compatibility equations and the integration of finite strains in two dimensions *Tectonophysics* **39**, T1-T6

Cobbold, P R 1979 Removal of finite deformation using strain trajectories *J Struct Geol* **1**, 67-72

Cobbold, P R 1980 Compatibility of two-dimensional strains and rotations along strain trajectories *J Struct Geol* **2**, 379–382

Cobbold, P R & Percevault, M N 1983 Spatial integration of strains using finite elements *J Struct Geol* **5**, 299–305

Cutler, J. M & Cobbold, P R 1985 A geometric approach to two dimensional finite strain compatibility. interpretation and review *J Struct Geol* **7**, 727-735

Etheridge, M A & Wilkie, J C 1981 An assessment of dynamically recrystallized grain size as a palaeopiezometer in quartz bearing mylonite zones *Tectonophysics* **38**, 475-508

Flinn, D 1962 On folding during three dimensional progressive deformation *Q J geol Soc Lond* **118**, 385–433

Fuller, G G & Leal, L G 1981 Flow birefringence of concentrated polymer solutions in two dimensional flows *J Polym Sci (Polym Phys Ed)* **19**, 557-587

Fung, Y C 1965 *Foundations of Solid Mechanics* Prentice Hall, Englewood Cliffs, New Jersey

Giesekus, H 1962 Stromungen mit konstantem Geschwindigkeitsgradienten und die Bewegung von darin suspendierten Teilchen Teil II Ebene Stromungen und eine experimentelle Anordnung zu ihrer Realisierung *Rheologica Acta* **2**, 112-122

Ghosh, S K 1987 Measure of non coaxiality *J Struct Geol* **9**, 111-113

Goetze, C & Evans, B 1979 Stress and temperature in the bending lithosphere as constrained by experimental rock mechanics *Geophys, J R astr. Soc* **59**, 463–478

Hobbs, B E, Means, W D. & Williams, P F 1976 *An Outline of Structural Geology* Wiley, New York

Jaeger, J C 1956 *Elasticity, Fracture and Flow* Chapman & Hall, London

Kuenen, P H 1965 Value of experiments in geology *Geol Mijnb* **44**, 22-36

Lisle, R J 1988 *Geological Strain Analysis—A Manual for the R_f/ϕ Method* Pergamon Press, Oxford

Lister, G S. & Williams, P. F 1983 The partitioning of deformation in flowing rock masses *Tectonophysics* **92**, 1-33

Malvern, L E 1969 *Introduction to the Mechanics of a Continuous Medium* (1st edn) Prentice Hall, Englewood Cliffs, New Jersey

Mason, S G 1977 Orthokinetic phenomena in disperse systems *J Colloid Interface Sci* **58**, 275–285

McKenzie, D P 1979 Finite deformation during fluid flow *Geophys J R astr Soc* **59**, 689–715

Means, W D 1976 *Stress and Strain* Springer, New York

Means, W D 1989 Stretching faults *Geology* **17**, 893–896

Means, W. D 1990 One dimensional kinematics of stretching faults *J Struct Geol* **12**, 267-272

Means, W D, Hobbs, B E, Lister, G S & Williams, P F 1980 Vorticity and non coaxiality in progressive deformation *J Struct Geol* **2**, 371-378

Passchier, C W 1986 Flow in natural shear zones—the consequences of spinning flow regimes *Earth Planet Sci Lett* **77**, 70–80

Passchier, C W 1987 Efficient use of the velocity gradients tensor in flow modelling *Tectonophysics* **136**, 159–163

Passchier, C W 1988 Analysis in deformation paths in shear zones *Geol Rdsch* **77**, 309–318

Passchier, C W 1990 A Mohr circle construction to plot the stretch history of material lines *J Struct Geol* **12**, 513–515

Pfiffner, O A & Ramsay, J G 1982 Constraints on geological strain rates arguments from finite strain states of naturally deformed rocks *J geophys Res* **87**, 311-321

Ramberg, H 1975a Particle paths, displacement and progressive strain applicable to rocks *Tectonophysics* **28**, 1-37 (see also Ramberg's (1986) correction in *Tectonophysics* **121**, 355)

Ramberg, H 1975b Superposition of homogeneous strain and progressive deformation in rocks *Bull geol Instn Univ Uppsala* **6**, 35–67

Ramberg, H 1986 Particle paths, displacement and progressive strain applicable to rocks—a correction *Tectonophysics* **121**, 355

Ramsay, J G 1967 *Folding and Fracturing of Rocks* McGraw Hill, New York

Ramsay, J G & Graham, R H 1970 Strain variation in shear belts *Can J Earth Sci* **7**, 786–813

Ramsay, J G & Huber, M. I 1983 *The Techniques of Modern Structural Geology, Volume 1 Strain Analysis* Academic Press, London

Ramsay, J G & Huber, M I 1987 *The Techniques of Modern Structural Geology, Volume 2 Folds and Fractures* Academic Press, London

Thompson, W & Tait, P G 1879 *Principles of Mechanics and Dynamics, Part* I (paperback version published 1962) Dover, New York

Tritton, D J 1988 *Physical Fluid Dynamics* (2nd edn) Clarendon, Oxford.

Truesdell, C 1953 Two measures of vorticity *J Rational Mech Anal* **2**, 173–217

Truesdell, C 1954 *The Kinematics of Vorticity* Indiana University Press, Bloomington, Indiana

Truesdell, C. 1965. *The Elements of Continuum Mechanics*. Springer, New York.

Truesdell, C. & Toupin, R. A. 1960. The classical field theories. In: *The Encyclopaedia of Physics* (edited by Flugge, S.). Springer, Heidelberg, 226–793.

Weijermars, R. 1986. Polydimethylsiloxane flow defined for experiments in fluid dynamics. *Appl. Phys. Lett.* **48**, 109–111.

Weijermars, R. 1988a. Convection experiments in high Prandtl number silicones, Part 2. Deformation, displacement and mixing in the Earth's mantle. *Tectonophysics* **154**, 97–123.

Weijermars, R. 1988b. Progressive deformation in low Reynolds number flow past a falling cylinder. *Am. J. Phys.* **56**, 534–540.

Weijermars, R. & Schmeling, H. 1986. Scaling of Newtonian and non-Newtonian fluid dynamics without inertia for quantitative modelling of rock flow due to gravity (including the concept of rheological similarity). *Phys. Earth & Planet. Interiors* **43**, 316–330.

APPENDIX A

MATHEMATICAL DESCRIPTION OF DEFORMATION

The changing position of any material body in flow space can be expressed as a relative displacement of material points. If an Eulerian description is adopted, the Cartesian position (x, y, z) of any point in displaced state had co-ordinates (x_0, y_0, z_0) before displacement. The rate of displacement $(\dot{x}_i)$ of particles x_i in Eulerian space (XYZ) can be described by the rate of displacement equation

$$\dot{x}_i = L_{ij}x_j \qquad \text{(A1)}$$

The rate-of-displacement or velocity gradient tensor L_{ij} $(= dv_i/dx_j)$ can be decomposed into a symmetric (stretching, strain rate, rate of deformation or velocity strain) tensor D_{ij} and an antisymmetric (vorticity, spin or rotation rate) tensor W_{ij} (Malvern 1969, p. 147)

$$L_{ij} = D_{ij} + W_{ij} \qquad \text{(A2)}$$

The stretching tensor implicitly describes the accumulation rate of incremental strain or strain rate. The vorticity tensor accounts for the rotation rate of the ellipsoid's principal axes.

In the case of homogeneous deformation, the stretching and vorticity tensors will comprise only linear terms

$$D_{ij} = (1/2)\left[\frac{dv_i}{dx_j} + \frac{dv_j}{dx_i}\right] = \begin{bmatrix} \dot{e}_{11} & \gamma_{12}/2 & \gamma_{13}/2 \\ \gamma_{21}/2 & \dot{e}_{22} & \gamma_{23}/2 \\ \gamma_{31}/2 & \gamma_{32}/2 & \dot{e}_{33} \end{bmatrix} \qquad \text{(A3)}$$

$$W_{ij} = (1/2)\left[\frac{dv_i}{dx_j} - \frac{dv_j}{dx_i}\right] = \begin{bmatrix} 0 & \omega_3/2 & -\omega_2/2 \\ -\omega_3/2 & 0 & \dot{\omega}_1/2 \\ \omega_2/2 & -\omega_1/2 & 0 \end{bmatrix}, \qquad \text{(A4)}$$

with vorticity vector components ω_k.

The particles started moving due to a deviatoric stress causing creep at a rate which is controlled solely by the internal friction or dynamic viscosity η of the material volume,

$$T_{ij} = 2\eta D_{ij}, \qquad \text{(A5)}$$

with deviatoric stress tensor T_{ij} and hydrostatic stress tensor $P_{ij} = -P\,\delta_{ij} = -1/3\sigma_{kk}\delta_{ij}$, taking $\delta_{ij} = 1$ for $i = j$ and $\delta_{ij} = 0$ for $i \neq j$. The boundary condition of plane strain requires that $\sigma_2 = P$ which implies $\sigma_2 = (1/2)(\sigma_1 + \sigma_3)$, so that

$$\begin{aligned} \tau_1 &= \sigma_1 - \sigma_2 = (1/2)(\sigma_1 - \sigma_3) \\ \tau_2 &= 0 \\ \tau_3 &= \sigma_3 - \sigma_2 = (1/2)(\sigma_3 - \sigma_1) \end{aligned} \qquad \text{(A6)}$$

This assumes that the deformation is incompressible, i.e. there is no volume change so that $\tau_1 = -\tau_3$. The difference in sign between τ_1 and τ_3 is accounted for by the opposite senses of the deviatoric stress arrows in Fig. 3.

The position of any particle at a particular time t can be found by integrating the set of differential equations (A1). This yields the deformation tensor F_{ij} which is equal to the sum of the Kronecker's matrix δ_{ij} and the displacement gradient tensor (du_i/dx_j), also termed the Jacobian matrix J_{ij} or the relative displacement matrix (cf. Malvern 1969, p. 124), $F_{ij} = J_{ij} + \delta_{ij}$. The solution of the integration may be expressed in terms of a relationship between the rate of displacement tensor L_{ij} and the deformation tensor F_{ij}. Assume L_{ij} and F_{ij} are given by the following matrices

$$L_{ij} = \begin{bmatrix} a & 0 & b \\ 0 & 0 & 0 \\ c & 0 & d \end{bmatrix} = \begin{bmatrix} a & b \\ c & d \end{bmatrix} \qquad \text{(A7)}$$

$$F_{ij} = \begin{bmatrix} A & 0 & B \\ 0 & 0 & 0 \\ C & 0 & D \end{bmatrix} = \begin{bmatrix} A & B \\ C & D \end{bmatrix} \qquad \text{(A8)}$$

The components A–D of the deformation matrix may be recovered from components a–d of the displacement rate matrix, but in a fashion much simpler than given by Ramberg (1975a,b). According to Ramberg (1975b, equation 43)

$$A = [(k_2 - a)/(k_2 - k_1)]\exp(k_1 t) - [(k_1 - a)/(k_2 - k_1)]\exp(k_2 t) \qquad \text{(A9)}$$

$$B = [(-b/(k_2 - k_1)][\exp(k_1 t) - \exp(k_2 t)] \qquad \text{(A10)}$$

$$C = [(k_1 - a)(k_2 - a)/(bk_2 - bk_1)][\exp(k_1 t) - \exp(k_2 t)] \qquad \text{(A11)}$$

$$D = [(k_2 - a)/(k_2 - k_1)]\exp(k_2 t) - [(k_1 - a)/(k_2 - k_1)]\exp(k_1 t) \qquad \text{(A12)}$$

The dummy constants k_1 and k_2 are (Ramberg 1975b, equation 34)

$$k_1 = (1/2)[(a + d) + \sqrt{[(a - d)^2 + 4bc]}] \qquad \text{(A13)}$$

$$k_2 = (1/2)[(a + d) - \sqrt{[(a - d)^2 + 4bc]}]. \qquad \text{(A14)}$$

This solution of F_{ij} is only valid if the square root contained in k_1 and k_2 is real, i.e. $[(a - d)^2 + 4bc] \geq 0$, which corresponds to cases of non-oscillatory deformation. If $[(a - d)^2 + 4bc] < 0$, this negative square root gives rise to complex eigenvalues, and alternative solutions valid for closed particle movement paths are given by Ramberg (1975b). However, it follows from expression (9c) that $c = 0$ in any plane, non-oscillatory deformation (but only for the reference frame used here), so that equations (A13) and (A14) yield $k_1 = a$ and $k_2 = d$. Substitution of these values in equations (A9)–(A12) gives the simplified solution for the components of the deformation matrix

$$A = \exp(at) \qquad \text{(A15)}$$

$$B = [b/(a - d)][\exp(at) - \exp(dt)] \qquad \text{(A16)}$$

$$C = 0 \qquad \text{(A17)}$$

$$D = \exp(dt) \qquad \text{(A18)}$$

It is worth recalling that in plane deformation $d = -a$, and $\exp(at) - \exp(-at) = 2\sinh(at)$. The streamline patterns for W_ks lying between 0 and 1 may be synthesized by alternating superposed increments of streamlines for pure and simple shear flow (see Ramberg 1975a, fig. 2).

Analogous to the rate of displacement tensor, the Jacobian displacement matrix, J_{ij}, can be separated—but only for infinitesimal deformations—into the sum of a symmetric matrix (E_{ij}) and skew symmetric matrix (Ω_{ij}) (Malvern 1969, p. 125)

$$J_{ij} = E_{ij} + \Omega_{ij} \qquad \text{(A19)}$$

The symmetric matrix describes the strain component of the deformation and is therefore called the strain matrix (Malvern 1969, p. 125)

$$E_{ij} = (1/2)\left[\frac{du_i}{dx_j} + \frac{du_j}{dx_i}\right] = \begin{bmatrix} e_{11} & \gamma_{12}/2 & \gamma_{13}/2 \\ \gamma_{21}/2 & e_{22} & \gamma_{23}/2 \\ \gamma_{31}/2 & \gamma_{32}/2 & e_{33} \end{bmatrix} \qquad \text{(A20)}$$

The rotation component of any deformation can be expressed by the rotation matrix (Malvern 1969, p. 131)

$$\Omega_{ij} = (1/2)\left|\frac{\partial u_i}{\partial x_j} - \frac{\partial u_j}{\partial x_i}\right| = \begin{bmatrix} 0 & \omega_3/2 & -\omega_2/2 \\ -\omega_3/2 & 0 & \omega_1/2 \\ \omega_2/2 & -\omega_1/2 & 0 \end{bmatrix}, \quad \text{(A21)}$$

with principal rotations ω_i. The above decomposition of the displacement matrix cannot be applied to finite strains, as non linear terms need to be taken into account for large deformations. However, Pfiffner & Ramsay (1982) have shown how finite strains may be determined by stepwise superposition of small increments of strain and rotation. The finite strains displayed in Figs. 5 and 6 were constructed from the particle movement paths after integration of the rate of displacement equations, which accounts for the non linearity of large deformations. It is worth noting that Ramsay & Huber (1983) sometimes used the term strain matrix for what is, in effect, the deformation matrix F_{ij}, since their matrix includes the rotation component of deformation.

APPENDIX B

SOFT SUPPORT FOR HARD ROCK DEFORMATION

A computer program has been written to calculate and display the progressive deformation of a unit volume of rock in ductile creep. The unit volume is homogeneously deformed, in plane isochoric strain. All parameters relevant to the progressive deformation history are quantified by the programme and may be printed if so required. The deformation stages are visualized by initially square and circular strain markers (e.g. Fig. 5). The movement paths of particular particles also can be displayed (e.g. Fig. 4). The rock may be either isotropic or orthotropic.

The graphical display of the strain markers has been programmed making efficient use of expressions (15)–(22). For example, the image of the strain ellipse is obtained according to the following procedure. The axial lengths of the major and minor axes of the ellipse, expressed as stretches S_1 and S_3, respectively, are given by equations (19a) and (19b), and (20a) and (20b). The inclination θ of the major axis with respect to the reference plane is given by expression (21). The co-ordinates of the strain ellipse (x,z) can first be obtained for an ellipse centred about the origin with its axes parallel to the reference frame

$$x = S_1 \cos\phi \quad \text{(B1)}$$

$$z = S_3 \sin\phi \quad \text{(B2)}$$

with dummy index $\phi = 0$–$360°$. The co-ordinates of the ellipse are subsequently rotated in the reference plane so that the ellipse inclines at angle θ with respect to the X axis.

$$x' = x\cos\theta - z\sin\theta \quad \text{(B3)}$$

$$z' = x\sin\theta + z\cos\theta \quad \text{(B4)}$$

The final co-ordinates of the ellipse for each deformation stage are obtained by translating the co-ordinates so that the ellipse remains centred in the deforming block.

The images of reciprocal strain are obtained, not by direct calculation, but by realizing that reciprocal strain caused by a stress oriented at ζ, is similar to progressive strain due to a stress oriented at $\zeta' = (90° - \zeta)$. The appropriate orientations of the reciprocal deformation stages are obtained by taking the mirror image about the Z axis.

All images are scaled automatically so that they remain within the field of view of the screen. This is achieved by scaling all co-ordinates in proportion to the maximum finite strain possible within the particular time scale, and under the stress/viscosity conditions specified by the user. Recall that values for rocks deforming in the lithosphere typically fall in the following orders of magnitude: 10–100 MPa for deviatoric stress, 5–10 Ma for tectonic episodes and 10^{21} – 10^{22} Pa s for effective viscosity of crustal rocks. The degree of orthotropy may be expressed by the anisotropy factor, which ranges from 1 for isotropic to ∞ for strongly orthotropic rocks (Weijermars in preparation).

The software was developed on a 2.9 kg Toshiba T1000 Laptop expanded with 768 kbytes battery buffered hard RAM. The final images of progressive deformation were displayed in screen mode 9 (640 × 350 pixels), using an IBM PS2 computer. Colours specified in the algorithms for the line drawings are blue (No. 1), grey (No. 8), red (No. 4) and green (No. 2), set against a black background (No. 0).

The photographs of Figs. 4 and 5 are taken from the 16 inch screen of an EIZO 9070S monitor assembled with MD B10 graphic card using an Olympus OM 10. The camera was mounted with 50 mm macro zoom lens (1: 3.5), and a tripod and remote control were used to trigger stable automatic exposure while compensating for the dark background by setting the filmspeed at higher values. The details in the images of Figs. 4 and 5 required use of Kodak EKTAR 25 film for superb resolution, setting filmspeed at 100 ASA. Prints were made with an automatic developer setting light intensity at fluxes 5 (Fig. 5) and 6 (Fig. 4).

The software, taking up only 16 kbytes of disk space and written in GWBASIC (81 kbytes), can be run on any IBM compatible PC or Laptop supported by DOS. Most of the graphics can be displayed sufficiently clearly if the hardware includes a CGA card. Optimum use of the graphical options can be made if the system is assembled with an EGA, VGA or Hercules graphics card to support colour display. Inquiries about the purchase of copies of the software together with detailed documentation may be obtained from the author.